

Reactive Interdiffusion between a Lead-Free Solder and Ti/Ni/Ag Thin-Film Metallizations

G. GHOSH

Northwestern University, Department of Materials Science and Engineering, Robert R. McCormick School of Engineering and Applied Science, Evanston, IL 60208. Email: g-ghosh@northwestern.edu

The reactive interdiffusion between a Sn-3.0wt.%Ag-0.7wt.%Cu solder and thin-film Ti/Ni/Ag metallizations on two semiconductor devices, a diode and a metal-oxide-semiconductor field-effect transistor (MOSFET), and a Au-layer on the substrates are studied. Comprehensive microanalytical techniques, scanning electron microscopy, transmission electron microscopy (TEM), and analytical electron microscopy (AEM) are employed to identify the interdiffusion processes during fabrication and service of the devices. During the reflow process of both diode and MOSFET devices, (1) the Ag layer dissolves in the liquid solder; (2) two intermetallics, $(\text{Ni,Cu})_3\text{Sn}_4$ and $(\text{Cu,Ni})_6\text{Sn}_5$, form near the back metal/solder interface; and (3) the Au metallization in the substrate side dissolves in the liquid solder, resulting in precipitation of the $(\text{Au,Ni,Cu})\text{Sn}_4$ intermetallic during solidification. During solid-state aging of both diode and MOSFET solder joints at 125°C and 200°C, the following atomic transport processes occur: (1) interdiffusion of Cu, Ni, and Sn, leading to the growth of a $(\text{Ni,Cu})_3\text{Sn}_4$ layer until the Ni layer is completely consumed; (2) interdiffusion of Au, Cu, Ni, and Sn through the $(\text{Ni,Cu})_3\text{Sn}_4$ layer and unconsumed Ni layer to the Ti layer to form a solid solution; and (3) further interdiffusion of Au, Cu, Ni, and Sn through the $(\text{Ni,Cu})_3\text{Sn}_4$ layer to form an $(\text{Au,Ti,Ni,Cu})\text{Sn}_4$ layer. The growth of the latter layer continues until the entire Ti layer is consumed.

Key words: Analytical electron microscopy (AEM), interfacial reaction, interdiffusion, intermetallic compounds, lead-free solder, transmission electron microscopy (TEM)

INTRODUCTION

Bare Si die can be attached to lead frames for use in packaged components or attached to circuit boards for use in chip-on-board (COB) applications using solders. The advantages of the COB approach is the reduction in circuit area required compared to using a packaged die. Furthermore, for power applications, the COB approach allows for the elimination of at least two interfaces that can act as paths of increased thermal resistance. The die can be attached using epoxy; "hard" solders, such as Au-3Si and Au-20Sn; or "soft" solders, such as low-melting Pb- and Sn-based solders. For power applications that require the dissipation of heat from the die, it is necessary to use one

of the solders, of which the soft solders are the most economical. For COB applications where the die is soldered directly to an organic circuit board, the only options are the Sn- or Pb-based solders, specifically those with a melting point well below 300°C because exposure to higher temperatures causes degradation of the organics in the circuit board. Therefore, it is desirable to use a solder with a melting point below 250°C, such as the eutectic Sn-Pb, Sn-Ag, Sn-Cu, or Sn-Ag-Cu solder.

Because of environmental concerns, it is becoming necessary to use Pb-free solders only in electronic packages. The fundamental issues that affect the microstructure of solder joints are back-side metallization, solder chemistry, details of the reflow process, and phase transformations in the solid state under the service conditions of a device. In many

(Received April 15, 2003; accepted July 2, 2003)

applications, the devices operate at the very high homologous temperature (≈ 0.9) of the solder. Under such conditions, extensive interdiffusion and phase transformations typically occur. These processes may have significant influence on the reliability of the devices through microstructural coarsening, thermal conductivity, heat capacity, ductile/brittle transition, and void formation, if any. Therefore, it has become necessary to start evaluating solder/back-metal reactions using Pb-free solders.

There have been some studies of the reactions between thin-film metallizations containing Ni as the solderable layer and different solder materials, including Sn-40Pb,¹⁻³ pure Sn,^{2,4} Sn-3.5Ag,³ and Sn-5Sb.³ Also, many studies^{2,5-9} have been conducted regarding the reactions between Sn-based solders and bulk or electroplated Ni.

Any Pb-free soft solder requires a solderable metallization to be present on the back of the Si die. However, such soft solders are known to react with various metallization schemes very rapidly in the liquid state and much more slowly in the solid state. A consequence of the interfacial reaction is the change in solder chemistry and microstructure of the solder joints that may have significant bearing on its mechanical properties. An example of a die back-side metallization is evaporated Ti/Ni/Ag. Here, the Ag layer preserves the solderability of the underlying Ni layer by limiting the oxidation at reflow temperature. In the absence of the Ag layer, the solderability of Ni is rather poor. The Ni layer serves as the solderable surface to which the joint is made. Ideally, it should be thick enough to prevent complete consumption to form the Ni-Sn intermetallic during reflow for the lifetime of a device at the service temperature. The Ti layer acts as an adhesion layer between the Ni layer and the Si die.

A schematic cross section of a diode solder joint, employing the Ti/Ni/Ag metallization scheme, is shown in Fig. 1. The metallization schemes (on the die side and the substrate side) along with the solder constitute a seven-component system (Au-Ag-Cu-Ni-P-Sn-Ti). Therefore, the microstructure of these solder joints after processing and the microstructural dynamics in service are expected to be quite complex. Furthermore, because of multilayer arrangement, the microstructural evolution is expected to be strongly time dependent because of the possibility of sequential phase formation. In view of these factors, a number of microanalytical tools may be needed to characterize the microstructure of solder joints and to understand the interdiffusion processes.

This work reports the results of a systematic study of dissolution and interfacial reactions between Sn-3.0Ag-0.7Cu (mass%) solder and the thin-film Ti/Ni/Ag metallizations on the die side. In our study, the die can be either a diode or a metal-oxide-semiconductor field-effect transistor (MOSFET). This work was performed with the following objectives: (1) to characterize the microstructure of solder joints after the reflow process and (2) to investigate

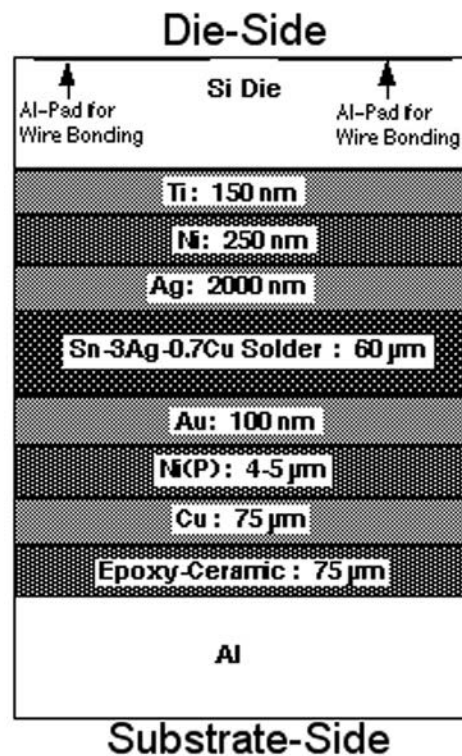


Fig. 1. Schematic diagram showing the cross section of a diode/solder joint.

the microstructural dynamics and the interdiffusion processes during solid-state aging of solder joints.

EXPERIMENTAL PROCEDURE

The diodes and the MOSFETs had back-side metallizations that were deposited by vacuum evaporation. The diodes had Ti/Ni/Ag as the back metal, with the Ti being in contact with the Si die, and the MOSFETs had Al/Ti/Ni/Ag as the back metal, with the Al being in contact with the Si die. The diode back-metal layer thicknesses were 0.15 μm , 0.25 μm , and 2 μm for the Ti, Ni, and Ag layers, respectively. The MOSFET back-metal layer thicknesses were about 0.15 μm , 1 μm , and 0.6 μm for the Ti, Ni, and Ag layers, respectively. The solder was in the form of 75- μm -thick preforms and had a nominal composition of Sn-3.0wt.%Ag-0.7wt.%Cu. The length and width of the preforms were matched to each of the diodes and MOSFETs. The diodes and MOSFETs were soldered to a substrate that had an electroless Ni(P) and immersion Au finish with thicknesses of 4 μm and 0.1 μm , respectively. The nominal P content in the electroless Ni was about 8 wt.%.

All the diode and MOSFET samples were soldered to the substrates in a N_2/H_2 atmosphere using a reflow process. The solder has a liquidus of about 220°C and stays liquid for about 8 min during reflow. The peak temperature of the reflow process is about 265°C. The as-reflowed joints were subsequently aged at 125°C for 200 h and 200°C for 20 h and 200 h.

The reflowed and aged samples were cut using a diamond saw and polished. Microstructural charac-

terization was carried out using a Hitachi (Hitachi, Ltd., Tokyo, Japan) S-4500 scanning electron microscope (SEM) equipped with a cold field-emission gun, a Princeton-Gamma Tech (Princeton-Gamma Tech, Inc., Princeton, NJ) energy-dispersive x-ray (EDX) detector, and the Integrated Microanalyzer for Imaging and x-ray software/database for composition analysis. The SEM was operated at 20 kV. Quantitative EDX technique is applied to characterize the interfacial phases when their sizes are sufficiently large ($>1 \mu\text{m}$). Conventional transmission electron microscopy (TEM) was carried out in a Hitachi 8100 microscope operated at 200 kV. The high-resolution analytical electron microscopy (AEM) was carried out in a Hitachi HF-2000 transmission electron microscope equipped with a Link EDX detector and data processor. The AEM was operated at 200 kV. A probe size of about 4 nm was used for diffraction and EDX experiments.

The thin foils of solder joints were prepared by dimpling and ion milling. The dimpling was carried out using a VCR (VCR Group, Inc., South San Francisco, CA) dimpler (Model D500i) to obtain specimens of about $10\text{-}\mu\text{m}$ thick, followed by ion milling in a Fischione (E.A. Fischione Instruments, Inc., PA, USA) Low Angle Milling and Polishing System (Model 1010) with a LN₂ cold stage. The specimen temperature was close to -196°C during the entire ion-milling process. To minimize the radiation induced damage/artifact, if any, in the beginning, an acceleration voltage of 4 kV was used, and it was gradually reduced to 2 kV with the progress of the milling process.

RESULTS

As-Deposited Ti/Ni/Ag Metallizations

As an example, Fig. 2a shows the SEM micrograph of as-deposited metal layers on the back side of a MOSFET. As seen, the back-metal layer thicknesses are $0.14 \mu\text{m}$, $1.1 \mu\text{m}$, and $0.6 \mu\text{m}$ for the Ti, Ni, and Ag layers, respectively. In the case of the diode, the back-metal layer thicknesses were determined to be $0.15 \mu\text{m}$, $0.25 \mu\text{m}$, and $2.1 \mu\text{m}$ for the Ti, Ni, and Ag layers, respectively.

Figure 2b and c shows the bright-field (BF) TEM micrographs of the as-deposited Ni and Ti layers on

the back side of a MOSFET. In the case of the Ni layer, both equiaxed and columnar grains with diameters of less than 50 nm are observed. In the case of the Ti layer, the grain size is always less than 25 nm. In both cases, convergent-beam electron diffraction experiments were carried out to confirm the fcc structure of Ni and the hexagonal close packed (hcp) structure of the Ti grains. Furthermore, the EDX spectra collected from these thin foils showed no evidence of interdiffusion between Ni, Ti, and Ag during the deposition process or any contamination during specimen preparation.

Scanning Electron Microscopy Investigation of Diode Metallization/Solder Interfacial Reaction

Figure 3a shows the joint between the diode back-side metallization and the solder. The thickness of the solder is about $55 \mu\text{m}$. After reflow, the bulk solder microstructure is fairly uniform; however, occasionally a few large Ag₃Sn dendrites (up to $30\text{-}\mu\text{m}$ long), emanating from both sides of the solder joints, are also observed. Figure 3b shows the microstructure near the die/solder interface. With respect to the back-side metallizations, the important results are (a) the Ag back-metal layer has dissolved completely in the solder during the reflow process; (b) the liquid solder reacts with the Ni layer to form intermetallics with at least three morphologies: small whiskers, equiaxed scallops, and faceted scallops; and (c) the Ni layer has been completely consumed during the reflow process. As a result, in some areas, the liquid solder comes in contact with the Ti layer. These areas are shown (marked X), as an example, in Fig. 3c.

The results of quantitative EDX analysis of the intermetallics, using the spot mode of the beam in the SEM, are listed in Table I. Figure 3b shows two chemically distinct types of intermetallics, IMC-I and IMC-II. The IMC-I particles are several microns in length, about $2\text{-}\mu\text{m}$ wide, highly faceted, and most are detached from the reaction interface. The EDX results strongly suggest that the IMC-I particles are the Ni₃Sn₄-type phase. The IMC-II particles are about $1\text{-}2 \mu\text{m}$ in dimension, equiaxed, and closer to the reaction interface. Based on EDX results, these

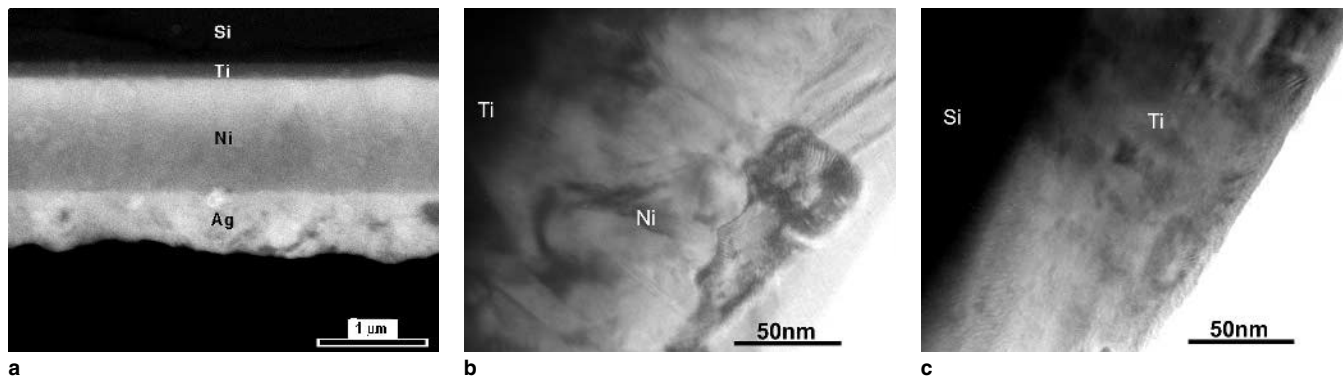


Fig. 2. (a) SEM micrographs of the as-deposited metallization scheme on the back side of a MOSFET. The BF TEM micrographs of a MOSFET metallization showing the grains of the (b) Ni layer and (c) Ti layer.

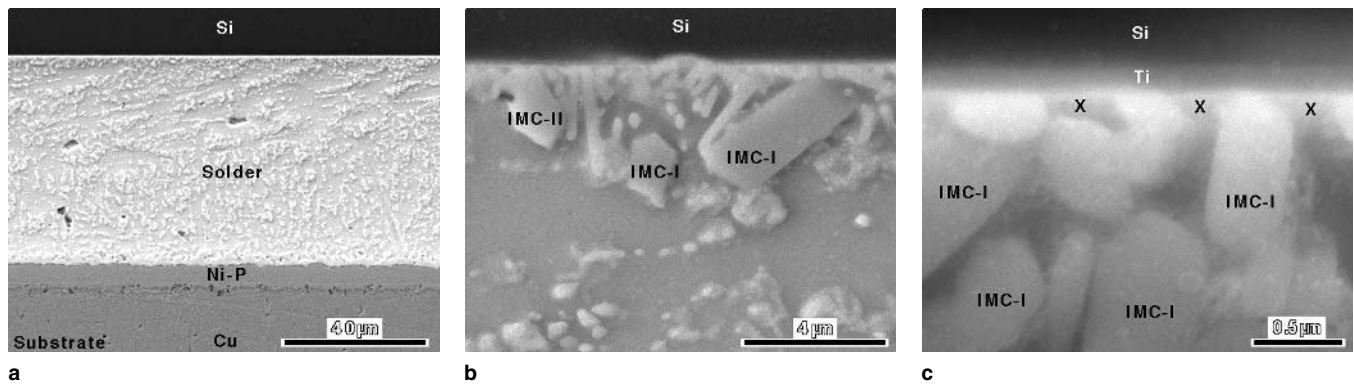


Fig. 3. SEM micrographs of the as-reflowed diode/solder joint: (a) showing the microstructure of the solder; (b) two types of IMCs near the interface: (i) small whiskers and faceted scallops of $(\text{Ni,Cu})_3\text{Sn}_4$ (IMC-I), and (ii) somewhat equiaxed $(\text{Cu,Ni})_6\text{Sn}_5$ phase (IMC-II); and (c) solder in contact with the Ti layer in the region marked X.

Table I. Composition of Ni_3Sn_4 -Type (IMC-I) and Cu_6Sn_5 -Type (IMC-II) Intermetallics in the Diode Solder Joints as a Function of Heat Treatment

Treatment	Composition of IMC-I (at.%)			Composition of IMC-II (at.%)		
	Cu	Ni	Sn	Cu	Ni	Sn
As-reflowed	7.08 ± 0.56	33.28 ± 1.45	59.64 ± 0.79	26.81 ± 1.85	22.54 ± 1.51	50.64 ± 1.61
125°C, 200 h	7.25 ± 1.06	33.56 ± 1.16	59.19 ± 1.05	29.31 ± 1.27	24.44 ± 1.13	46.24 ± 0.77
200°C, 20 h	7.56 ± 0.64	34.09 ± 1.45	58.34 ± 0.73	29.86 ± 0.75	23.93 ± 0.87	46.21 ± 0.63
200°C, 200 h	5.83 ± 0.95	35.07 ± 1.61	59.11 ± 0.71	29.65 ± 1.12	23.35 ± 1.47	47.00 ± 0.81

are believed to be the Cu_6Sn_5 -type phase. The Ag content in both types of intermetallic compounds (IMCs) was negligible. The dimension of the small whiskers, shown in Fig. 3b and c, precludes the possibility of accurate composition analysis using the SEM/EDX technique. It should be noted that the Cu layer on the substrate side is completely buried under the Ni(P) layer (Fig. 3a); therefore, all the Cu found in the IMCs originates from the Cu in the solder.

In Fig. 3c, the spalling of very small whiskers, which are typically 0.2–0.5 μm in diameter, is seen. The reactive diffusion between Ni and the liquid solder involves several processes, including grain-boundary grooving of the intermetallic by the liquid solder. This along with the residual stress in thin films may have caused spalling of Ni_3Sn_4 at such small length scales.

The important microstructural dynamics during solid-state aging are (1) the coarsening of dispersed (after reflow) IMCs and (2) the interfacial reaction involving the Ti layer. An interesting observation is that the faceted scallops of IMC-I undergo coarsening along with the small whiskers. This suggests that the small whiskers are also Ni_3Sn_4 , but they are too small for composition analysis by the SEM/EDX technique. Two types of interfacial reactions, involving the Ti layer, were observed during solid-state aging.

Figure 4a and b shows the interfacial microstructures of diode solder joints after aging at 125°C for 200 h and at 200°C for 20 h, respectively. In these microstructures, even though the Ti layer is completely shielded by the IMC-I grains, it is evident

that the Ti layer has reacted. However, the extent of reaction is rather nonuniform along the interface. Some areas showed no reaction with the Ti layer, while other areas, such as area A in Fig. 4a and b, show complete consumption of the Ti layer in intermetallic formation. It is also obvious that the reaction always starts at the Ti/IMC-I interface, and the reaction front moves toward the Ti/Si interface. X-ray mapping in the SEM showed the depletion of Ti and the presence of Sn in what used to be the Ti layer, which will be discussed further. The similarity of the microstructures in Fig. 4a and b, with respect to the Ti layer, indicates that at the initial stages the fundamental interdiffusion mechanism leading to these microstructures is the same for the two different aging conditions with the interdiffusion kinetics being slower at the lower temperature.

The other Ti layer reaction occurred in areas where the IMC-I grains had spalled away from the die back metal, exposing the Ti to the solder, as shown in Fig. 3c. In this case, the reaction between the solder and the Ti layer, during the aging at 200°C for 20 h, yielded a somewhat uniform and a thicker layer of intermetallic, as shown in Fig. 4c. Figure 4d shows further growth during prolonged aging at 200°C for 200 h, causing complete consumption of the Ti layer. The EDX spectrum, collected in the spot mode of the electron beam and x-ray mapping of this layer, indicated that the primary constituents in this layer are Au, Sn, and Ti. It is interesting to note that the average thickness of the Au-Sn-Ti layer is about 0.75 μm , which is about 5 times thicker than the as-deposited Ti layer. It is worth pointing out that the origin of Au is (1) disso-

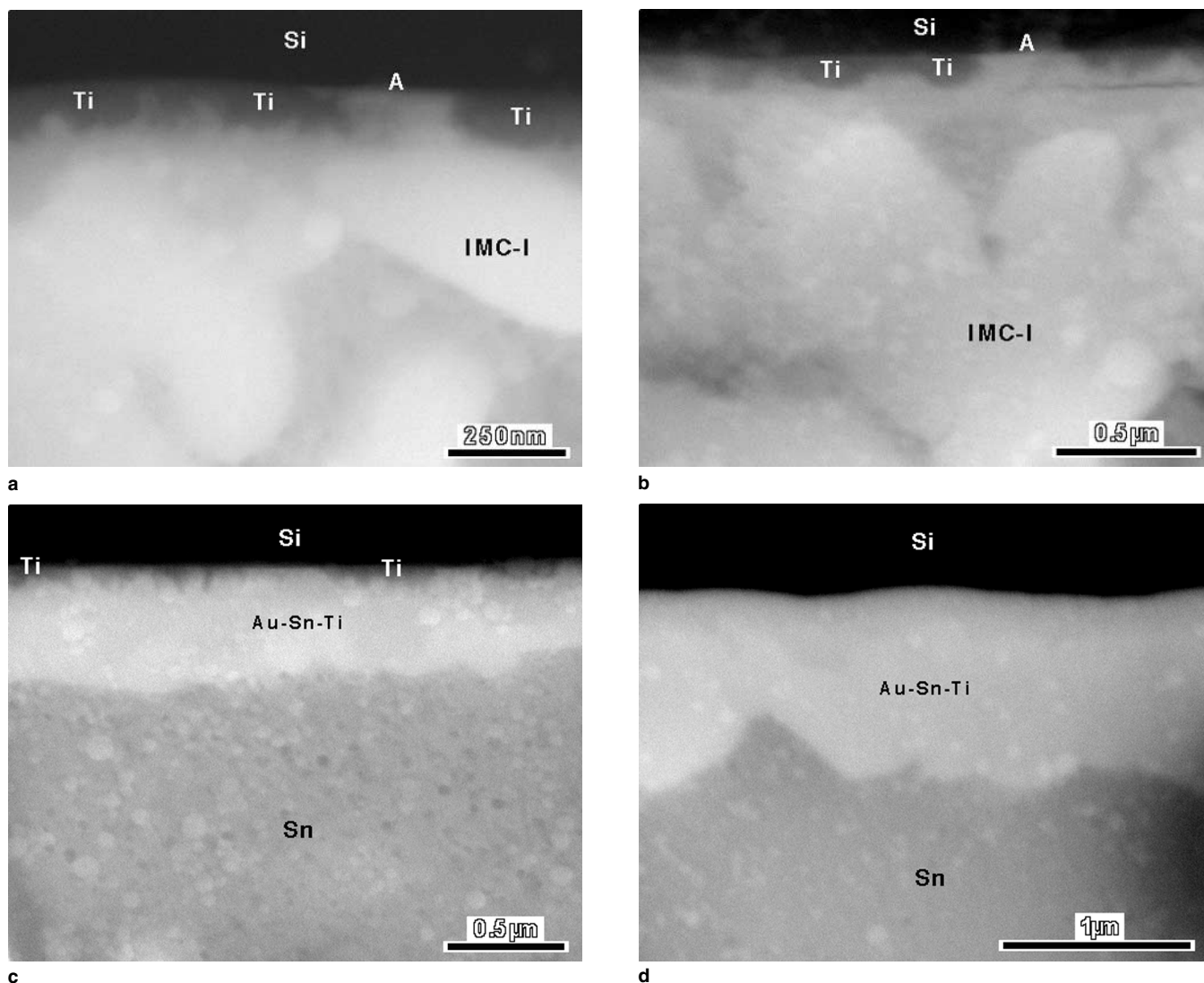


Fig. 4. Interfacial microstructures (SEM) after solid-state aging of a diode/solder joint: (a) at 125°C for 200 h, showing partial reaction of the Ti layer; (b) at 200°C for 20 h, showing partial reaction of the Ti layer; (c) at 200°C for 20 h (another region), showing the formation of a continuous layer of Au-Sn-Ti in contact with Sn and also the consumption of most of the Ti layer; and (d) at 200°C for 200 h, showing complete reaction of the Ti layer and further growth of the Au-Sn-Ti layer relative to that in (c).

lution of Au on the substrate metallization in the liquid solder during reflow and (2) the migration of Au from the bulk solder to the IMC/solder interface.

The compositions of the two intermetallics, IMC-I and IMC-II, are listed in Table I as a function of aging treatment. The composition of IMC-I is independent of heat treatment. However, after the aging treatment, the IMC-II phase is further enriched with about 3at.%Cu and depleted by about 3at.%Sn.

Scanning Electron Microscopy Investigation of MOSFET Metallization/Solder Interfacial Reaction

Figure 5a shows the joint between the MOSFET back-side metallization and the solder. The thickness of the solder is about 75 μm. After reflow, the bulk solder microstructure is fairly uniform. Like the diode metallization/solder case, the Ag layer dissolved completely in the liquid solder. As shown in Fig. 5b, irregular-shaped scallops near the MOSFET/solder

interface are present. The composition of these relatively large and irregular scallops, labeled IMC-I, is shown in Table II. The results of quantitative EDX analysis show that these scallops are Ni_3Sn_4 . The overall composition and the nature of Cu partitioning on the Ni sublattice are very similar to those observed in the case of diode/solder joints. Besides the isolated scallops, a three-dimensional skeleton-like microstructure, involving the intermetallic and solder, was also observed. An example of this interfacial microstructure is shown in Fig. 5c. The inner part of the skeleton microstructure consists of a continuous layer of IMC-I. The composition of this continuous layer was also identified as being Ni_3Sn_4 . Figure 5c also shows that the Ni layer was not completely consumed during the reflow process. The average thickness of the unconsumed Ni layer is about 0.5 μm, but is rather nonuniform despite the fact that the as-deposited Ni layer in the MOSFET back-side metallization was uniform in thickness.

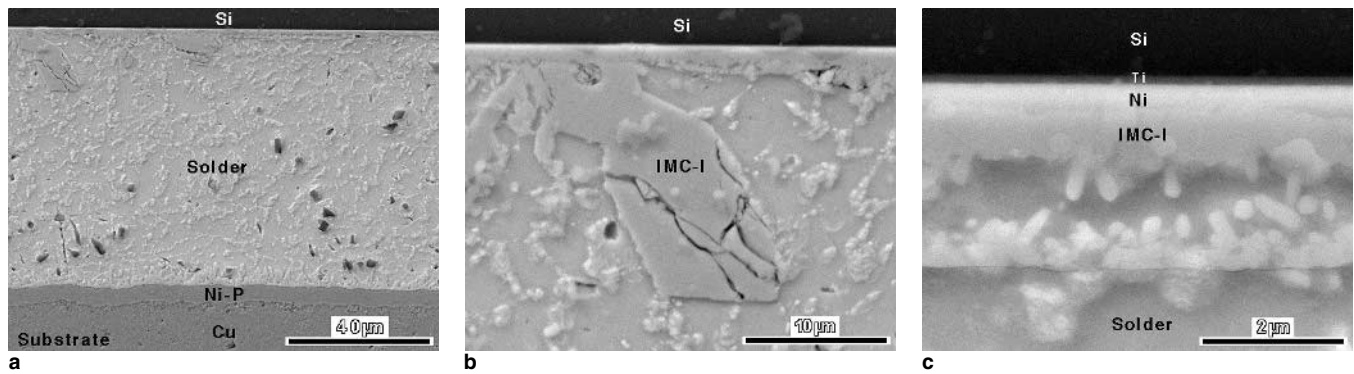


Fig. 5. SEM micrographs of the as-reflowed MOSFET/solder joint: (a) showing the whole solder joint, (b) showing a large and isolated scallop of $(\text{Ni,Cu})_3\text{Sn}_4$ (IMC-I), and (c) skeleton morphology of $(\text{Ni,Cu})_3\text{Sn}_4$ (IMC-I) and nonuniform thickness of the unconsumed Ni layer.

Table II. Composition of Isolated Ni_3Sn_4 -Type (IMC-I) Scallops and the Ni_3Sn_4 -Type Layer (IMC-I) in the MOSFET Solder Joints as a Function of Heat Treatment

Treatment	Composition (at.%) of Isolated Ni_3Sn_4 -Type Scallops (IMC-I)			Composition (at.%) of the Ni_3Sn_4 -Type Layer (IMC-I)		
	Cu	Ni	Sn	Cu	Ni	Sn
As-reflowed	6.88 ± 0.96	34.07 ± 0.72	59.06 ± 0.54	4.78 ± 1.18	37.25 ± 3.45	57.97 ± 1.37
125°C, 200 h	5.69 ± 1.10	36.46 ± 1.02	57.85 ± 0.42	5.34 ± 2.10	37.21 ± 2.09	57.45 ± 0.86
200°C, 20 h	6.51 ± 0.83	34.56 ± 1.2	58.93 ± 0.79	4.37 ± 1.08	35.98 ± 0.89	59.65 ± 0.56
200°C, 200 h	6.16 ± 0.77	35.44 ± 0.79	58.40 ± 0.40	4.85 ± 1.18	36.17 ± 0.75	58.97 ± 0.28

The important microstructural dynamics during solid-state aging at 200°C are (1) similar to the diode solder joints, Ni_3Sn_4 scallops coarsened from the as-reflowed condition; (2) the reactions between Ni and Sn resulted in significant growth of the Ni_3Sn_4 layer, (3) similar to the as-reflowed MOSFET solder joint, the thickness of the Ni_3Sn_4 layer was nonuniform and, at some places, the original Ni layer has been completely consumed; and (4) at the areas where the Ni has been completely consumed because of the formation of Ni_3Sn_4 , two continuous layers of intermetallics, Ni_3Sn_4 and Au-Sn-Ti, are observed during aging at 200°C.

A nonuniformity of the unconsumed Ni layer after reflow causes a nonuniformity of the interfacial microstructure during subsequent solid-state aging. Figure 6a and b shows the interfacial microstructures after aging at 200°C for 20 h. Figure 6a shows that in the presence of the unconsumed Ni layer, the Ti layer is protected from any interfacial reaction. As a result, the thickness of the Ti layer is the same as that after vacuum evaporation. After the same aging treatment, we also find areas, an example is shown in Fig. 6b, where the entire Ni layer has been consumed to form Ni_3Sn_4 , causing the formation of an Au-Sn-Ti layer. As a result, the thickness of the Ti layer has decreased (on the average) by about 25%. These results show that the unconsumed Ni layer acts as a good diffusion barrier for Au.

Figure 6c shows coarsening of dispersed Ni_3Sn_4 scallops after aging at 200°C for 200 h. However, the dominant mechanism of coarsening is by physical coalescence, a process caused by anisotropic mass

flow and the formation of growth neck(s) between two or more particles. For example, scallops 1 and 2 and scallops 3, 4, and 5 in Fig. 6c are undergoing coalescence. This phenomenon is commonly observed during the liquid-phase sintering process with a very high volume fraction of the solid phase. Figure 6d shows the interfacial microstructure of the MOSFET/solder joint after aging at 200°C for 200 h. Here, the Ti layer is completely consumed resulting in further growth of the Au-Sn-Ti intermetallic layer relative to that in Fig. 6b. This microstructural observation is identical to that observed in the diode solder joint after the same aging treatment. Also, the average thickness of the Au-Sn-Ti intermetallic layer after aging at 200°C for 200 h is very similar in both the diode and MOSFET solder joints.

The compositions of Ni_3Sn_4 scallops and the Ni_3Sn_4 continuous layer were determined by EDX analysis in the SEM, and the results are listed in Table II as a function of aging treatment. They differ slightly with respect to the Cu and Ni content, with the scallops having about 2 at.% more Cu than the layer. However, for a given morphology, the composition is independent of aging treatment.

TEM/AEM Investigation of MOSFET Metallization/Solder Interfacial Reaction

To establish the fundamental interdiffusion processes controlling the dynamics of the interfacial microstructure of solder joints, in particular, the reactions involving the Ti layer, thin foils of solder joints were examined by TEM/AEM. Our goal was not to quantify the interdiffusion processes, rather

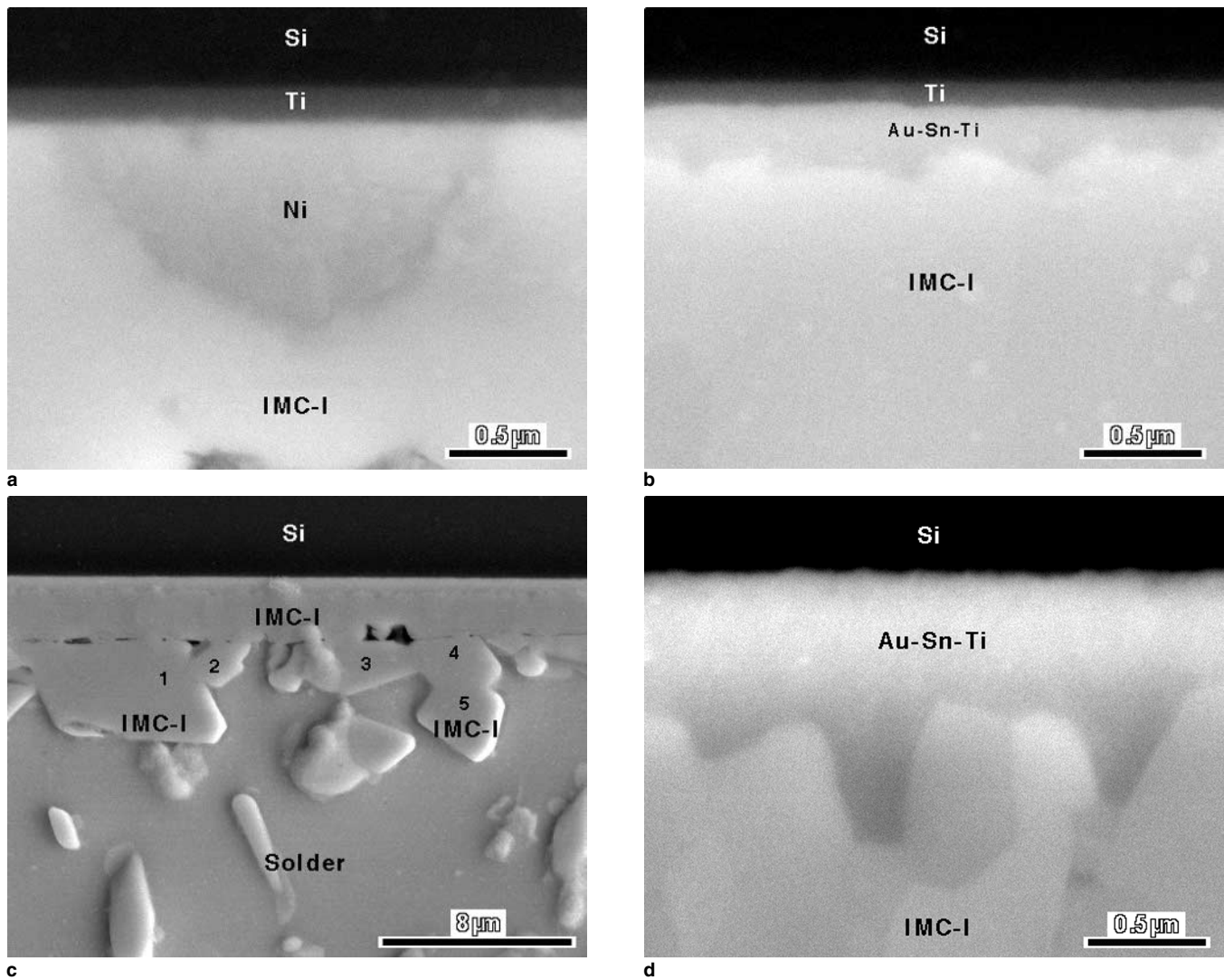


Fig. 6. Interfacial microstructures (SEM) after solid-state aging of a MOSFET/solder joint: (a) at 200°C for 20 h, showing the protection of the Ti layer because of the presence of the unconsumed Ni layer; (b) another region in the same sample as in (a) showing the absence of a Ni layer and partial consumption of the Ti layer to form a continuous layer of Au-Sn-Ti; (c) at 200°C for 200 h, showing coarsening of $(\text{Ni,Cu})_3\text{Sn}_4$ scallops; and (d) at 200°C for 200 h, showing complete reaction of the Ti layer and further growth of the Au-Sn-Ti layer relative to that in (b).

to qualitatively establish interdiffusion processes. The aforementioned SEM results demonstrate that the reactive interdiffusion during reflow and the microstructural dynamics during solid-state aging are the same in both diode and MOSFET solder joints. Therefore, as an example, in the following, we present the results of the TEM/AEM investigation for the MOSFET solder joints that were aged at 200°C for 200 h. After this aging treatment, both the Ni and Ti layers react to form intermetallics, as shown in Fig. 6, despite the fact that the Ni layer in the MOSFET back metal is much thicker compared to the diode back metal.

Figure 7 shows the BF TEM micrograph of the solder. A large number of rod-shaped precipitates along with a few dendritic precipitates, identified as Ag_3Sn , are observed. The rod-shaped Ag_3Sn precipitates are about 200 nm in length and 30 nm in diameter. In thin foils, because of the sectioning effect,

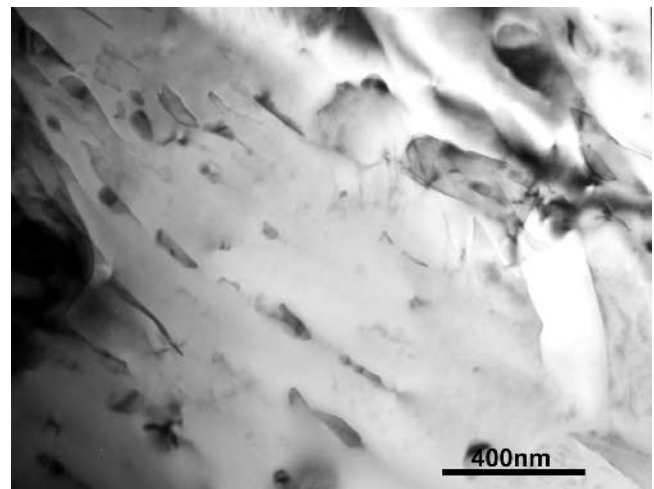


Fig. 7. BF TEM micrograph of the solder showing Ag_3Sn precipitates in the Sn matrix.

the dendritic Ag_3Sn particles are about 500 nm in length and 100 nm in diameter even though they appear much larger in the SEM micrographs.

In addition to Ag_3Sn , several AuSn_4 particles were also observed in the thin foils even though they were not detected in the SEM micrographs. These particles are blocky and irregular in shape. Particles with and without internal defects, such as twins and stacking faults, were observed. As an example, Fig. 8a is the BF TEM micrograph of an AuSn_4 particle exhibiting many internal defects. Several transmission electron diffraction patterns (DPs) were collected from the same particle by tilting the foil in the transmission electron microscope. The DPs are found to be consistent with the known crystallographic data of the AuSn_4 phase. Two DPs of AuSn_4 along the [130] and [121] zone axes are shown in Fig. 8b and c, respectively. Two EDX spectra collected from two AuSn_4 particles dispersed in solder are shown in Fig. 8d and e, of which Fig. 8d corresponds to the particle shown in Fig. 8a. These EDX spectra clearly underscore the presence of variable amounts of Cu and Ni in AuSn_4 , with Cu content being much less than the Ni content.

Figure 9a shows the BF TEM micrograph corresponding to the continuous intermetallic layer (IMC-I) in Fig. 6c, which was identified as Ni_3Sn_4 through the SEM/EDX technique. As seen in Fig. 9a, the Ni_3Sn_4 layer consists of polyhedral grains that are less than 1 μm in diameter. Once again, several

DPs were obtained by tilting the foil in the transmission electron microscope, which confirmed the structure of this intermetallic. Two DPs of Ni_3Sn_4 along the [001] and [021] zone axes are shown in Fig. 9b and c, respectively. The results presented earlier (with respect to Figs. 4c and d and 6d) imply that Au has to diffuse through the Ni_3Sn_4 layer to form the Au-Sn-Ti phase. Therefore, it is essential to establish that, at the aging temperatures, Ni_3Sn_4 has indeed some solubility of Au, however, small it may be; otherwise, the Ni_3Sn_4 layer should act as an ideal diffusion barrier, which is certainly not the case. The EDX spectra were also obtained from several Ni_3Sn_4 grains in the layer. A representative EDX spectrum, shown in Fig. 9d, demonstrates that the Au content in Ni_3Sn_4 is barely detectable.

The BF TEM micrographs, corresponding to the Au-Sn-Ti layer in Fig. 6d, are shown in Fig. 10a and b. Numerous polyhedral and elongated grains with diameters less than 100 nm are seen. Also, the long axis of the elongated grains always lies in the plane of the interface. Analysis of the DPs taken from the nanoscale grains confirms that they have the same structure as the AuSn_4 phase. Figure 10c shows the DP of the elongated grain shown in Fig. 10b along the [210] zone axis, and the corresponding EDX pattern is shown in Fig. 10d. Gold, tin, and a significant amount of titanium along with some copper and nickel are also present in this phase. It is very interesting to note that the Ti peak is always absent

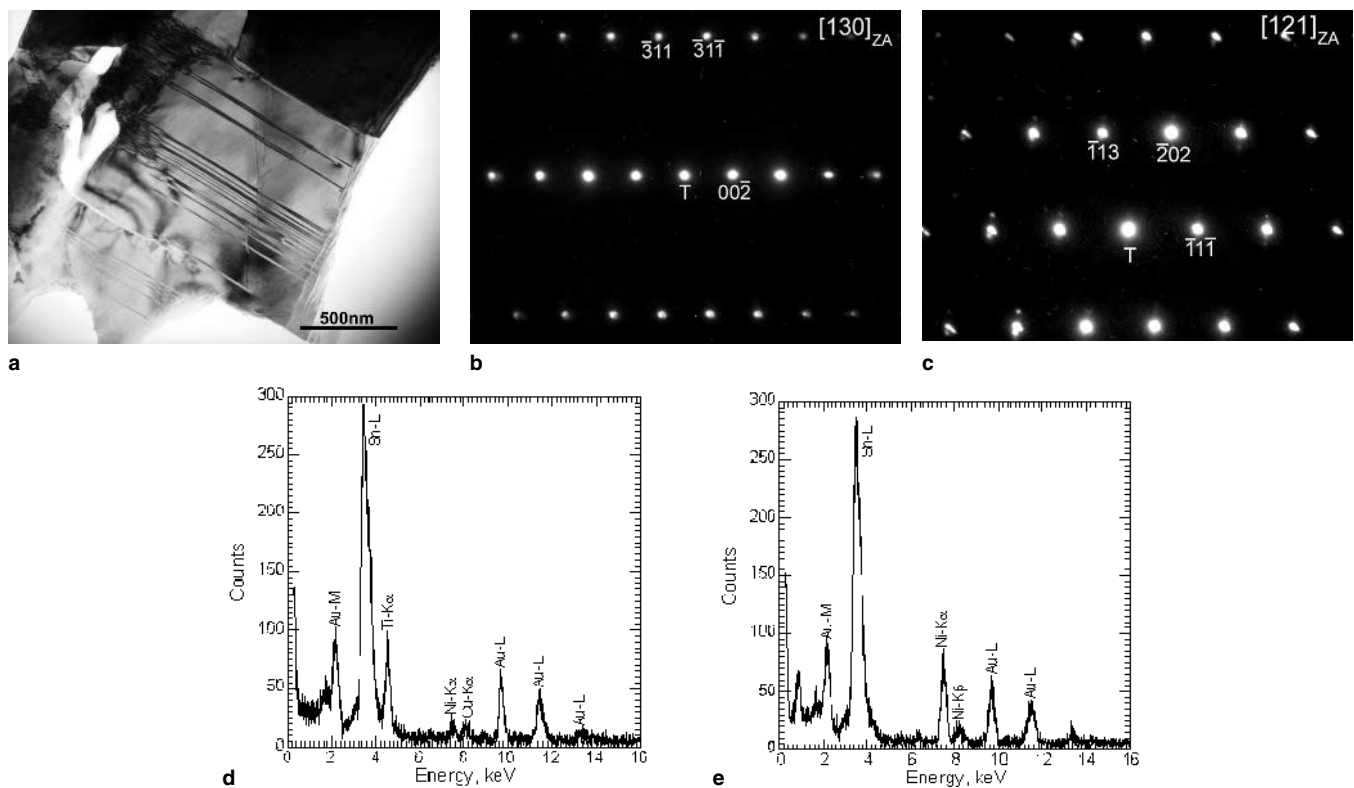


Fig. 8. (a) BF TEM micrograph showing a AuSn_4 particle containing many internal defects; (b) and (c) DPs from the AuSn_4 particle shown in (a) along [130] and [121] zone axes, respectively; and (d) and (e) EDX spectra showing variation in Ni and Cu contents in the AuSn_4 phase and the absence of a Ti peak.

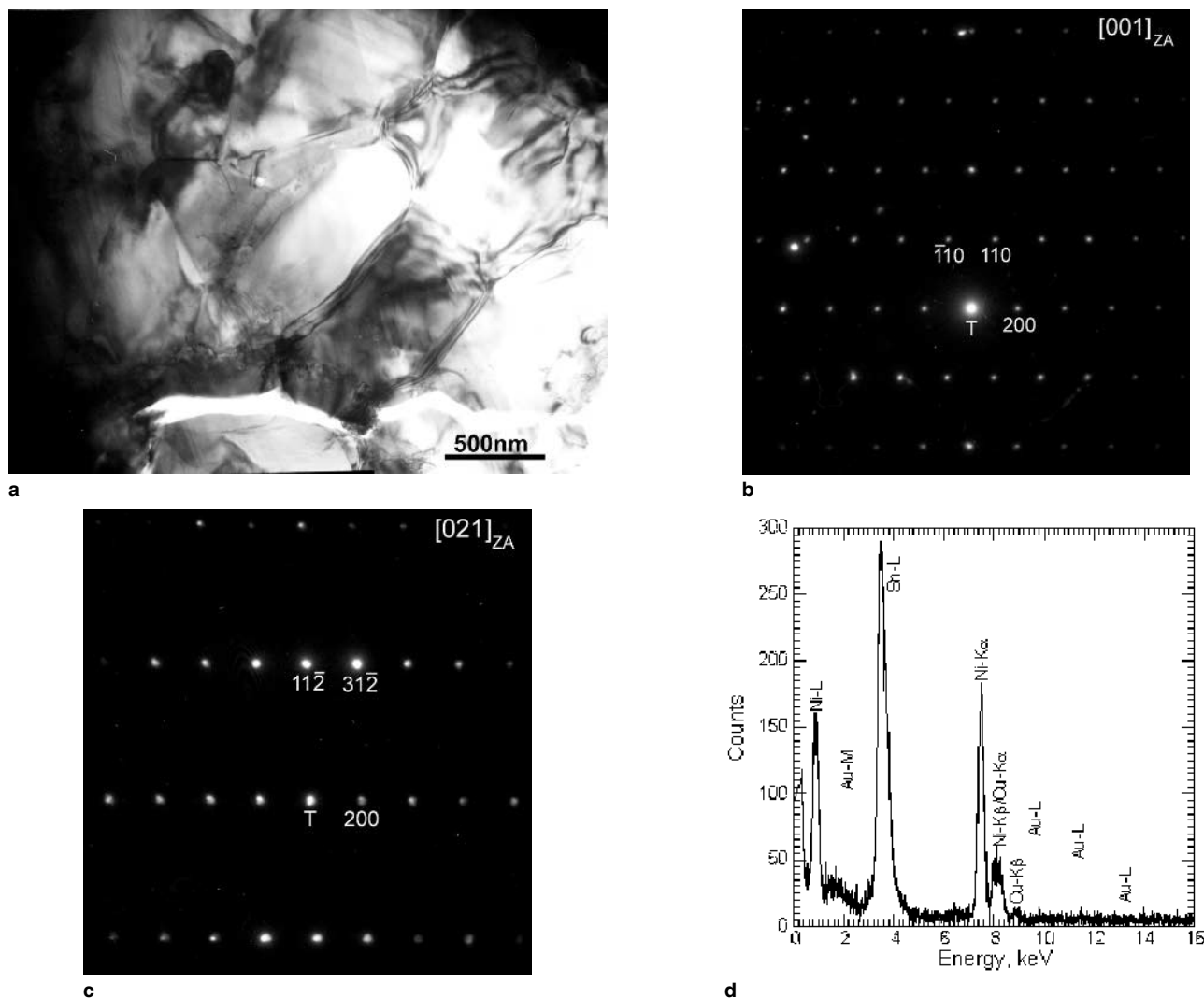


Fig. 9. (a) BF TEM micrograph showing $(\text{Ni,Cu})_3\text{Sn}_4$ grains in the IMC-I layer shown in Fig. 6d; (b) and (c) DPs from $(\text{Ni,Cu})_3\text{Sn}_4$ along $[001]$ and $[021]$ zone axes, respectively; and (d) EDX spectra showing that Au in $(\text{Ni,Cu})_3\text{Sn}_4$ is barely detectable.

in the EDX spectra of AuSn_4 particles in the solder, shown in Fig. 8d and e, and also in the EDX spectrum of Ni_3Sn_4 , shown in Fig. 9d. These results suggest that Ti does not diffuse to the solder side.

A closer examination of the thin foils revealed the presence of patches of unreacted Ti that was less than 50 nm in thickness; however, such areas were difficult to see in the SEM micrographs, where it appeared that the entire Ti layer was consumed (Fig. 6d). An example of unreacted Ti is shown as a BF TEM micrograph in Fig. 10b. A corresponding DP is shown in Fig. 11a, confirming the structure to be hcp. Once again, EDX spectra taken from several unreacted Ti grains provide valuable clues about the interdiffusion processes prior to the formation of the $(\text{Au,Ti,Ni,Cu})\text{Sn}_4$ intermetallic. Figure 11b and c shows the EDX spectra demonstrating variation of Au, Cu, Ni, and Sn in the Ti grains. In the EDX spectra, it was always found that an increase in Sn intensity, relative to Ti intensity, was associated with the relative increase in intensity of Au, Cu, and Ni. Such variations simply indicate the extent

of interdiffusion. Also, their presence in hcp Ti demonstrate the formation of a solid solution prior to the formation of the $(\text{Au,Ti,Ni,Cu})\text{Sn}_4$ intermetallic. We believe that the bright areas marked A in Fig. 6a and b, where the Ti layer appears to have reacted, correspond to the formation of the solid solution.

The presence of Au, Cu, Ni, and Sn in Ti grains, detected in the EDX spectra of thin foils, and their variations should not be considered as an experimental artifact caused by the proximity of the Ti grains to the $(\text{Au,Ti,Ni,Cu})\text{Sn}_4$ intermetallic. The electron probe size (≈ 4 nm) used to collect the EDX spectra is much smaller than the grain size.

DISCUSSION

Bader¹⁰ reported a rapid dissolution of Ag in liquid solder. In our experiments, the complete dissolution of the Ag layer may be rationalized based on thermodynamic argument alone. In the reflow process, the peak temperature reaches up to 265°C. A simple calculation shows that the dissolution of the 2- μm -thick

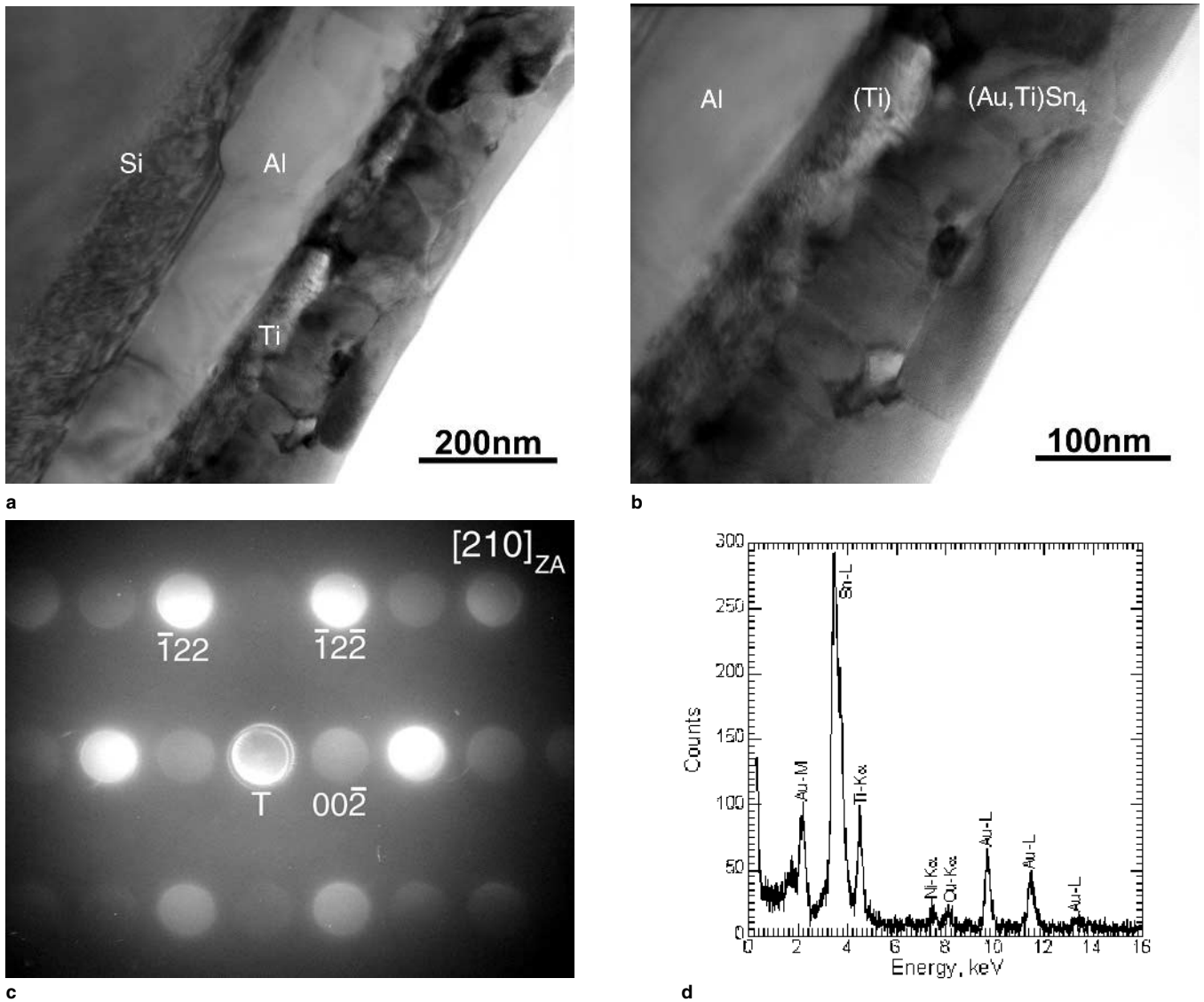


Fig. 10. (a) BF TEM micrograph showing numerous (Au,Ti,Ni,Cu)Sn₄ grains in the Au-Sn-Ti layer shown in Fig. 6d, (b) untransformed Ti grains, and (c) DP from (Au,Ti,Ni,Cu)Sn₄ along [210] zone axis; and (d) EDX spectrum from (Au,Ti,Ni,Cu)Sn₄.

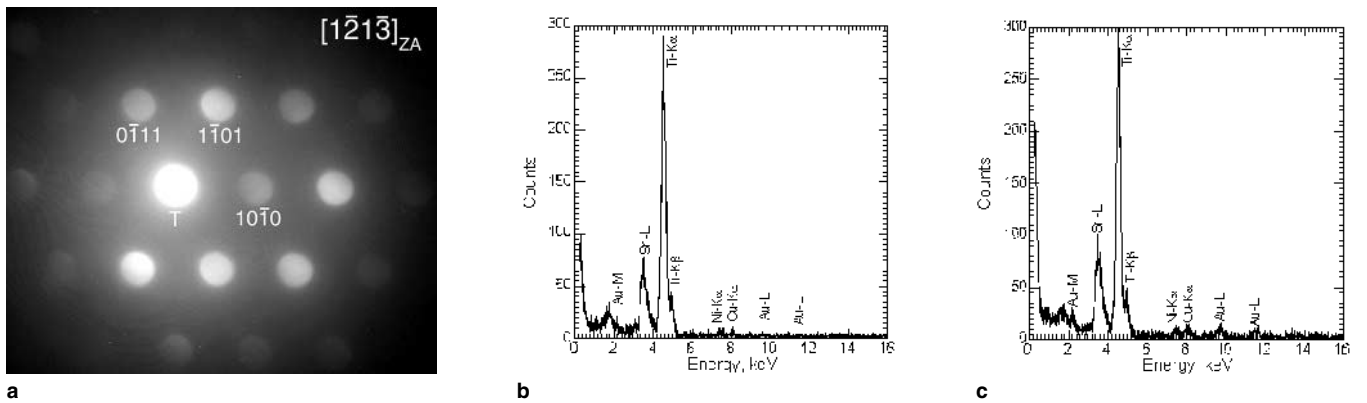


Fig. 11. (a) DP from untransformed Ti grains shown in Fig. 10b; and (b) and (c) EDX spectra showing variations in Au, Cu, Ni, and Sn contents in Ti grains.

Ag layer in a 60- μ m-thick solder in the case of the diode joint and the dissolution of the 0.6- μ m-thick Ag layer in the case of the MOSFET joint increase

the Ag content of solder from 3 mass% to about 5.8 mass% and 3.7 mass%, respectively. These are below the solubility limit (with respect to Ag₃Sn) of

Table III. Crystallographic Data of the Intermetallic Phases Observed in This Study

Phase [Ref.]	Pearson Symbol, Space Group (No.), Prototype	Atomic Positions	Lattice Parameter (nm)	Comments
Ag ₃ Sn [12]	oP8, Pmmn (59), Cu ₃ Ti	Ag1 (2b): 0 0.5 0.8277 Ag2 (4f): 0.75 0 0.6631 Sn (2a): 0 0 0.1687	a = 0.59689 b = 0.47802 c = 0.51844	—
AuSn ₄ [13]	oC20, Aba2 (41), PtSn ₄	Au (4a): 0 0 0 Sn1 (8b): 0.1639 0.3395 0.1205 Sn2 (8b): 0.1312 0.1642 0.8591	a = 0.65124 b = 0.65162 c = 1.17065	Cu, Ni, and Ti mix randomly on the Au sublattice
Cu ₆ Sn ₅ [14]	hP4, P6 ₃ /mmc (194), AsNi	M1 (2a): 0 0 0 M2 (2c): 0.6667 0.3333 0.25	a = 0.41922 c = 0.50372	Ni mixes randomly on the Cu sublattice
Ni ₃ Sn ₄ [15]	mC14, C2/m (12), Ni ₃ Sn ₄	Ni1 (2a): 0 0 0 Ni2 (4i): 0.2147 0 0.3369 Sn1 (4i): 0.4286 0 0.6864 Sn2 (4i): 0.1718 0 0.8123	a = 1.22146 b = 0.40602 c = 0.51293 β = 105°	Cu mixes randomly on the Ni sublattice

6.9 mass% at 265°C. Therefore, the experimental observations are consistent with the equilibrium phase diagram. Furthermore, a comprehensive diffusional simulation, taking nonlinear heating during reflow into account, also predicts complete dissolution of the Ag layer in the liquid solder.¹¹

Table III summarizes the crystallographic data^{12–15} of the intermetallic phases observed in this study. The compositions of Cu₆Sn₅ and Ni₃Sn₄ listed in Tables I and II are in good agreement with previous reports.^{16–18} Even though the overall composition of these phases is not a direct measure of the distribution of Cu (or Ni) atoms between Ni (or Cu) and Sn sublattices, we strongly believe that the Ni atoms reside on the Cu sublattice and vice versa in the cases of Cu₆Sn₅ and Ni₃Sn₄, respectively. This may be explained in terms of experimental thermodynamic data that showed that Cu-Sn and Ni-Sn bonds are stronger than the Cu-Ni bonds. This causes a preferential partitioning of Cu to the Ni sublattice, allowing for a minimum energy configuration by maximizing the number of Cu-Sn bonds. Hence, we represent these phases as (Cu,Ni)₆Sn₅ and (Ni,Cu)₃Sn₄.

A similar argument is also applicable to AuSn₄. The EDX spectra shown in Figs. 8d and e and 10d suggest that substantial amounts of Cu, Ni, and Ti dissolve in AuSn₄, and it is likely these elements reside primarily on the Au sublattice even when all are present simultaneously. In fact, it is well established that Ni can replace up to 50% of the Au sites in AuSn₄ forming (Au_{0.5}Ni_{0.5})Sn₄.^{19–21} Accordingly, we represent the Au-Sn-Ti layer as (Au,Ti,Ni,Cu)Sn₄.

A surprising result is the formation of the (Au,Ti,Ni,Cu)Sn₄ layer behind the (Ni,Cu)₃Sn₄ layer at temperatures of 125°C and 200°C in both diode and MOSFET solder joints. Notwithstanding the presence of the (Au,Ni,Cu)Sn₄ phase in the solder, in the case of the MOSFET solder joints, Au has to be transported through the (Ni,Cu)₃Sn₄ layer to form (Au,Ti,Ni,Cu)Sn₄. The fairly rapid transformation kinetics of (Au,Ti,Ni,Cu)Sn₄ implies that either the

solubility of Au in (Ni,Cu)₃Sn₄ is high, the diffusivity of Au in (Ni,Cu)₃Sn₄ is high irrespective of its solubility, or both. As shown in Fig. 9d (the EDX spectrum collected from a (Ni,Cu)₃Sn₄ grain that was in contact with an (Au,Ni)Sn₄ grain), the Au content in (Ni,Cu)₃Sn₄ is barely detectable. Minor and Morris²² also reported that the Ni₃Sn₄ intermetallic at the interface of the solder joints contains very little Au. However, to our knowledge, this is first time the formation of the Ti-bearing AuSn₄ IMC having complex chemistry is reported.

Based on the aforementioned results, we postulate that Au diffuses rather fast in the Ni₃Sn₄ layer. However, at this time, there is no experimental data on the lattice diffusivity of Au in Ni₃Sn₄ to corroborate our assertion. We also postulate that grain-boundary diffusion of Au in (Ni,Cu)₃Sn₄ may give rise to fairly rapid growth kinetics of the (Au,Ti,Ni,Cu)Sn₄ layer. This mechanism may be justified based upon two premises. First, the (Ni,Cu)₃Sn₄ layer consists of small grains, less than 1 μm in diameter, as shown in Fig. 9a, that form during solid-state aging. Second, the maximum aging temperature of 473 K represents a low (<0.5) homologous temperature, T/T_m, with T_m being taken as the peritectic temperature (1,066 K) as a lower limit of the melting point of Ni₃Sn₄. These factors are known to promote the grain-boundary diffusion mechanism.

As mentioned earlier, combined transmission electron diffraction experiment and EDX analysis confirm the formation of a hcp solid solution of Ti, containing variable amounts of Au, Cu, Ni, and Sn. According to the Ti-X (X = Au, Cu, Ni, and Sn) phase diagrams,²³ the solvus boundaries extrapolated to 473 K suggest that while the equilibrium solid solubility of Sn in hcp Ti is about 5 at.%, that of Au, Cu, and Ni is almost negligible. Yet, the EDX spectra collected from Ti grains suggest that Au, Cu, and Ni contents are significant. This apparent discrepancy may be attributed to two factors. First, the equilibrium solubility in the Ti-X (X = Au, Cu, Ni) phase diagrams is with respect to the corresponding inter-

metallic phase, whereas, in this study, the EDX spectra are collected from Ti grains in contact with the (Au,Ti,Ni,Cu)Sn₄ intermetallic. In other words, the (Au,Ti,Ni,Cu)Sn₄ intermetallic may be thermodynamically less stable compared to the Ti-X intermetallics that determine equilibrium solid solubility. Second, the prevailing thermodynamic and kinetic constraints in solder joints may represent a metastable state.

CONCLUSIONS

A comprehensive microstructural study is performed employing a SEM, TEM, and AEM to investigate the reactive interdiffusion between thin-film Ti/Ni/Ag metallization and the Sn-3.0Ag-0.7Cu solder. The following conclusions are drawn.

- In both diode/solder and MOSFET/solder joints, the Ag layer dissolves during the reflow process.
- In the solder joints, two intermetallics are found near the back metal/solder interface: (Ni,Cu)₃Sn₄, and (Cu,Ni)₆Sn₅.
- During the solid-state aging of solder joints, the primary microstructural dynamics are (1) coarsening of (Ni,Cu)₃Sn₄ scallops and short whiskers; (2) interdiffusion of Cu, Ni, and Sn, leading to growth of the ((Ni,Cu)₃Sn₄ layer; (3) interdiffusion of Au, Cu, Ni, and Sn from solder to Ti layer to form a hcp solid solution; and (4) further interdiffusion of Au and Sn through the (Ni,Cu)₃Sn₄ layer leads to the formation of the (Au,Ti,Ni,Cu)Sn₄ intermetallic layer, which grows until all Ti is consumed. However, there was no evidence of Ti diffusing to the (Ni,Cu)₃Sn₄ layer or into the solder.
- Our results clearly demonstrate that it is possible to form intermetallics containing Ti at temperatures that actual electronic products will be exposed to during normal operation.
- We postulate that a grain-boundary diffusion mechanism of Au through the (Ni,Cu)₃Sn₄

layer governs the growth kinetics of the (Au,Ti,Ni,Cu)Sn₄ layer.

ACKNOWLEDGEMENTS

The financial support from the National Science Foundation (Grant No. DMR-9813919) and Motorola is gratefully acknowledged.

REFERENCES

1. H.N Keller, *IEEE Trans. CHMT* 19, 433 (1986).
2. S.K. Kang, R.S. Rai, and S. Purushothaman, *J. Electron. Mater.* 25, 1113 (1996).
3. P.G. Kim, J.W. Wang, T.Y. Lee, and K.N. Tu, *J. Appl. Phys.* 86, 6746 (1999).
4. S. Bader, W. Gust, and H. Heiber, *Acta Metall. Mater.* 43, 329 (1995).
5. S.K. Kang and V. Ramachandran, *Scripta Metall.* 14, 421 (1980).
6. W.K. Choi and H.M. Lee, *J. Electron. Mater.* 28, 1251 (1999).
7. G. Ghosh, *Acta Mater.* 48, 3719 (2000).
8. G. Ghosh, *J. Electron. Mater.* 29, 1182 (2000).
9. G. Ghosh, *J. Appl. Phys.* 88, 6887 (2000).
10. W.G. Bader, *Welding J., Res. Suppl.* 48, 551-s (1969).
11. G. Ghosh, *Acta Mater.* 49, 2609 (2001).
12. C.W. Fairhurst and J.B. Cohen, *Acta Cryst., Sec. B* 28B, 371 (1972).
13. R. Kubiak and M. Wolcyrz, *J. Less-Common Met.* 97, 265 (1984).
14. A. Gangulee, G.C. Das, and M.B. Bever, *Metall. Trans.* 4, 2063 (1973).
15. W. Jeitschko and B. Jabor, *Acta Cryst., Sec. B* 38B, 598 (1982).
16. J.Y. Park, C.W. Yang, J.S. Ha, C.-U. Kim, E.J. Kwon, S.B. Jung, and C.S. Kang, *J. Electron. Mater.* 30, 1165 (2001).
17. A. Zribi, A. Clark, L. Zavalij, P. Borgensen, and E.J. Cotts, *J. Electron. Mater.* 30, 1157 (2001).
18. C.-H. Lin, S.-W. Chen, and C.-H. Wang, *J. Electron. Mater.* 31, 907 (2002).
19. C.E. Ho, R. Zheng, G.L. Guo, A.H. Lin, and C.R. Kao, *J. Electron. Mater.* 29, 1175 (2000).
20. A. Zribi et al., *IEEE Trans. Comp. Packaging Technol.* 23, 383 (2000).
21. A. Minor and J.W. Morris, Jr., *Metall. Mater. Trans. A* 31, 798 (2000).
22. A. Minor and J.W. Morris, Jr., *J. Electron. Mater.* 29, 1170 (2000).
23. T.B. Massalski, ed., *Binary Alloy Phase Diagrams*, Vols. 1–3 (Materials Park, OH: ASM International, 1990).